

pubs.acs.org/IECR Review

Synthesis and Application of Magnetic Nanocrystal Clusters

Zhen Xiao, Linlin Zhang, Vicki L. Colvin, Qingbo Zhang,* and Gang Bao*



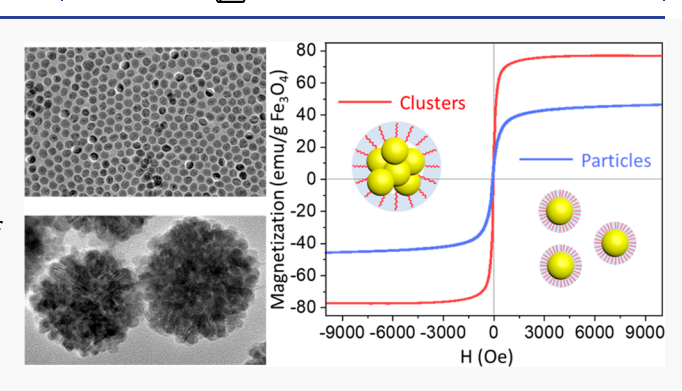
Cite This: Ind. Eng. Chem. Res. 2022, 61, 7613-7625



ACCESS |

III Metrics & More

ABSTRACT: Magnetic nanocrystal clusters exhibit unique properties that differ from the constituent nanocrystals due to the intracluster interactions. This Review summarizes the recent advances in the synthesis and application of magnetic nanocrystal clusters. Specifically, we describe the formation mechanism of the clusters, discuss the strategies to control the dimensions of the clusters and primary nanocrystals, and showcase the applications of clusters in magnetic hyperthermia cancer therapy, magnetic resonance imaging, drug delivery, wastewater treatment, and the formation of photonic crystals. The opportunities and challenges in improving magnetic nanocrystal clusters for different applications are also discussed.



Article Recommendations

I. INTRODUCTION

When the dimension of magnetic materials is reduced to a specific size, the magnetization of particles can randomly flip direction because of the thermal fluctuation. This phenomenon is called superparamagnetism. Superparamagnetic nanocrystals can be magnetized quickly in an external magnetic field, and the magnetization disappears when the magnetic field is removed. The superparamagnetism of nanocrystals is usually manifested by the zero remanence and coercivity in the magnetization curve. Because of their interesting properties, superparamagnetic nanocrystals remain a rich source of scientific inquiry and technological exploration. They have found many applications in a wide variety of fields, such as wastewater treatment, oil reservoir imaging, drug delivery, and hyperthermia for cancer treatment.

Extensive efforts have been made to generate magnetic nanocrystals of different sizes and determine their sizedependent properties. 10-13 It has been demonstrated that wet chemistry offers a powerful tool to generate uniform nanocrystals dispersed in solutions. 14-17 Many solution chemistry methods have been developed to synthesize an extensive library of magnetic nanocrystals with different sizes and compositions. These nanocrystals have enabled researchers to establish the relationship between particle size and magnetic properties and explore their uses in a wide variety of applications. 18-21 It was found that big nanocrystals exhibit better performance than smaller ones in many applications since the big magnetic moments make the particles more susceptible to the external magnetic field. ^{22–26} An increase in nanocrystal size, however, will cause an increase in the anisotropy energy of the particles. The increased anisotropy energy will block the thermal fluctuation of the magnetic

moment, as manifested by their increased coercivity and remanence. The nanocrystals in the blocked state have a tendency to aggregate in the solution, thus compromising their functionalities in many applications. $^{30-33}$

Recently, it was found that the properties of magnetic nanomaterials can be further modified by clustering nanocrystals into controlled aggregates.^{34–37} Each aggregate, or cluster, consists of tens to thousands of small single nanocrystals.^{38–43} The magnetic properties of clusters may dramatically differ from those of constituent particles due to the interaction between particles. 35,44 For example, the cluster can retain superparamagnetism at a much bigger size than isolated nanocrystals. 45,46 Because of these different properties, nanocrystal clusters display much better performance in some applications.³⁴ Since the properties of clusters are dependent on the dimensions of both clusters and primary particles, it is crucial to control these two structural parameters for the establishment of structure-property relationship and achievement of optimal performance for a specific application. The synthesis of magnetic nanocrystal clusters has drawn the attention of many researchers, and many methods have been reported to control the size of the cluster and primary particle. The nanocrystal clusters are usually synthesized using either two-step self-assembly or one-step polyol synthesis, as shown in Figure 1.47,48

Special Issue: Jim Yang Lee Festschrift

Received: December 13, 2021 Revised: February 4, 2022 Accepted: February 9, 2022 Published: February 17, 2022





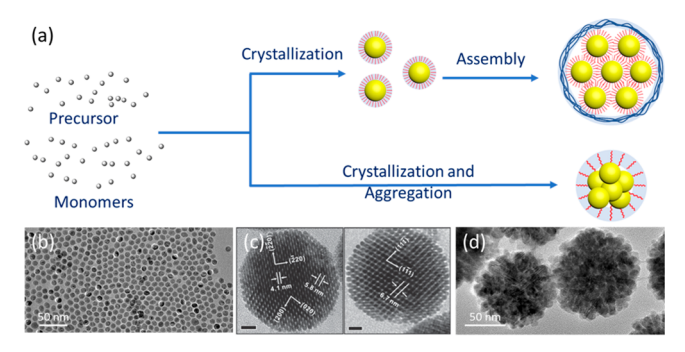


Figure 1. The synthesis of magnetic nanocrystal clusters. (a) Schematic illustration of the one-pot method and two-step method to generate clusters. (b) TEM images of isolated magnetic nanocrystals. (c) Clusters formed via the two-step method. [Figure adapted from ref 38 with permission. Copyright 2007, American Chemical Society, Washington, DC.] (d) Clusters formed via one-pot synthesis.

In this Review, we examine the recent advances in the synthesis and application of magnetic nanocrystal clusters. We focus our discussion on the clusters synthesized using the one-pot method, since this method is efficient to control the dimensions of the cluster. We begin the discussion with the formation mechanism of magnetic nanocrystal clusters, followed by the summary of the effort to control the cluster size and primary particle size, the unique magnetic properties of the clusters, and the application of magnetic nanocrystal clusters in various fields. We conclude this article with an outlook for the future research directions of magnetic nanocrystal clusters, including the opportunities and challenges.

II. THE FORMATION MECHANISM OF MAGNETIC NANOCRYSTAL CLUSTERS

The ferrite magnetic nanocrystal clusters were usually synthesized by the thermo-decomposition of the metal salts. In a typical synthesis of clusters, a metal precursor, a capping agent, and an alkaline substance are mixed in a polyol solvent. The metal precursor undergoes forced hydrolysis reactions and reductions at high temperatures and turns into monomers of the nanocrystals (metal oxide), which eventually form the clusters. While iron precursors may undergo self-hydrolysis in many solutions, the forced hydrolysis at a very high rate is essential for the formation of uniform magnetic nanocrystal clusters. The most common reactants are summarized in Table 1. By changing the nature and concentration of the reactants, the reaction time, and the reaction temperature, clusters consisting of tens to thousands of nanocrystals could be generated. 49,50 The magnetic nanocrystal clusters are generally deemed to follow a two-step formation mechanism. In the first step, primary nanocrystals are formed through nucleation and growth, as indicated by the conventional LaMer mechanism. These primary nanocrystals then aggregate to form clusters. The aggregation of the primary nanocrystals to form clusters might follow different pathways, depending on the reaction system and conditions. The detailed mechanism of the cluster formation is still unclear.

Metal oxide nanocrystal clusters might be formed through limited ligand protection (LLP), first proposed by Narayanaswamy et al. (Figure 2). S1 They found that isolated In_2O_3 nanocrystals were formed when the amount of ligands was

much higher than that of the metal precursor, while clusters (nanoflowers) were formed when the amount of ligand was significantly decreased. The nanocrystals formed in the reaction had a tendency to group together to reduce their surface areas until the desired ligand:surface ratio is achieved if the amount of ligand is insufficient and the primary nanocrystals cannot be fully protected during the nanocrystal formation. The ligand:surface ratio also accounts for the surprisingly high uniformity of the clusters. In principle, the LLP mechanism could account for the formation of clusters composed of other metal oxides, such as iron oxide.

Many researchers found that clusters could be formed even if there is a sufficient amount of capping agents in the reaction solution. The formation of the clusters might be because of the competition between the attractive force and the repulsive force, as suggested by Cheng et al. The primary particles assume high surface tension, which makes them have a tendency to aggregate. Meanwhile, the capping agent binds to the particle surface, which provides the electrostatic and/or steric repelling force. The balance between these two opposite driving forces might account for the formation of clusters and determine the cluster dimension.

The clusters could be formed via the ligands' cross-linking of the primary nanocrystals. Wei et al. synthesized magnetite nanocrystal clusters using diethylene glycol as the solvent and reducing agent. They attributed the formation of clusters to the dicarboxylic acids, the oxidative product of diethylene glycol (Figure 3).⁵⁹ The dicarboxylic acids could cross-link the primary particles to form clusters. If triethylene glycol (TEG) or tetraethylene glycol (TTEG) were used as the solvent and reducing agent instead of diethylene glycol, only particles were observed as the oxidative product of TEG or TTEG cannot interconnect the primary particles. In another work, Togashi et al. synthesized magnetite nanocrystal clusters using 3,4dihydroxyhydroxycinnamic acid (DHCA) as the capping agent. Both the phenolic hydroxyl groups and the carboxylic groups in DHCA can form dative bonds with iron, thus interconnecting primary nanocrystal to clusters.60

The clusters might undergo Ostwald ripening once the reaction is complete, which leads to the change of the cluster morphology. In the synthesis of isolated nanocrystals, Ostwald ripening leads to the growth of big particles at the expense of small particles. In the clusters, Ostwald ripening usually causes the increase of the primary particles. Gerber et al. monitored the formation process of magnetite nanocrystal clusters using high-resolution TEM (HRTEM) (Figure 4a). They found that the diameter of the primary particles could increase from 5 to 25 nm if the reaction time increased from 7 to 13 h while the cluster diameter remained 250 nm. Gavilan et al. found a similar phenomenon in the generation of maghemite nanocrystal clusters (Figure 4b). Both TEM images and X-ray diffraction (XRD) spectra clearly show that the primary particles increase dramatically with reaction time.

III. SYNTHESIS OF THE MAGNETIC NANOCRYSTAL CLUSTERS WITH CONTROLLED DIMENSIONS

Synthesis of the clusters with controlled dimensions is challenging, since there are two parameters to control: cluster size and primary particle size. In principle, the size of the cluster and primary particles can be controlled by varying the nature and concentration of the reactants, the reaction time, and the reaction temperature. The relationship between the reaction conditions and the kinetics of nucleation, growth,

Table 1. Summary of One-Step Approaches for Magnetic Cluster Synthesis

reference	composition	capping agent	alkaline	solvent	reaction temp (°C)	reaction method	size range	size control
Cheng ⁴⁷ (2011)	Fe ₃ O ₄ /Fe ₂ O ₃ mixed phase	succinic acid	urea	ethylene glycol (EG) and 1,2-propylene gly- col (PG)	200	hydrothermal	varying cluster diameter 50–300 nm	solvent ratio and reaction time
Gavilan ⁵⁸ (2017)	Fe_3O_4	polyvinylpyrrolidone (PVP40)	sodium acetate	EG	200	hydrothermal	cluster diameter at 60 nm, varying grain size from 11 nm to 24 nm (XRD)	reaction time
Ge ⁴⁵ (2007)	Fe_3O_4	poly(acrylic acid) (PAA)	sodium hydrox- ide	diethylene glycol (DEG)	220	NaOH injection	varying cluster diameter 30–180 nm, nanocrystal size at 6 nm	NaOH concentration
Hemery ⁶³ (2017)	γ -Fe ₂ O ₃ (oxidized by nitrate)	N/A	sodium hydrox- ide	EDG and N-methyldie- thanolamine (NMDEA)	220	thermal decom- position	varying cluster diameter 10–50 nm	water content
Kostopoulou ⁶⁴ (2014)	γ -Fe $_2$ O $_3$	PAA	sodium hydrox- ide	DEG	220	NaOH injection	cluster diameter 50 and 85 nm	water content in solvent with different grade
Lin ⁶² (2013)	Fe_3O_4	ethylenediaminetetracetic acid disodium (EDTA Na2)	sodium acetate	EG	180-200	hydrothermal	varying cluster diameter 100–260 nm, nanocrystal size at 6 nm	different time of sonication pretreatment
Maity ⁶⁵ (2011)	Fe_3O_4	N/A	iron(III) acetyla- cetonate	tri(ethylene glycol) (TREG) and triethanolamine (TREA)	245-280	thermal decom- position	cluster diameter 44 nm	TREG and TREA ratio
Nikitin ⁶⁶ (2018)	Fe_3O_4	series of organic acid	N/A	benzyl ether and 1,2- hexadecanediol	210-260	thermal decom- position	varying cluster diameter 20–40 nm	using different ligand in the synthesis
Otero-Lorenzo ⁶¹ (2017)	Fe_3O_4 and $Mn_xFe_{3-x}O_4$	polyethylene glycol	sodium acetate	EG	185	hydrothermal	varying cluster diameter 30–180 nm, nanocrystal size at 7 nm	reaction time
Xuan ⁶⁷ (2009)	$\mathrm{Fe_3O_4}$	polyvinylpyrrolidone (PVP, K30)	sodium acetate, sodium acryl- ate	EG and DEG	200	hydrothermal	varying cluster diameter 6–280 nm, varying nanocrystal size 6–14 nm	cluster diameter controlled by EG/DEG ratio; nanocrystal size controlled by acetate/acrylate ratio
Cheng ⁴⁸ (2009)	Fe_3O_4	sodium citrate	urea	EG	200	hydrothermal	varying cluster diameter 40–300 nm	amount of sodium citrate
$\operatorname{Gerber}^{57}(2017)$	Fe_3O_4	succinic acid	urea	EG	200	hydrothermal	varying cluster diameter 100–250 nm, varying nano- crystal size 3–25 nm	reaction time
Huang ⁶⁸ (2016)	Fe_3O_4	PEG-2000, hexadecyltrimethyl ammonium bromide (CTAB)	sodium acetate	EG, DEG, PG, and triethylene glycol (TEG)	200	hydrothermal	varying cluster diameter 55–480 nm	ratio of solvent
Lartigue ⁴⁴ (2012)	γ -Fe ₂ O ₃ (oxidizing Fe ₃ O ₄ by nitrate)	N/A	sodium hydrox- ide	EDG and NMDEA	220	thermal decom- position	varying cluster diameter 10–30 nm	ratio of solvent
Liang ⁶⁹ (2013)	Fe_3O_4	PAA and sodium dodecyl benzenesulfonic (SDBS)	sodium acetate	EG	200	hydrothermal	varying cluster diameter 200–400 nm	amount of PAA or SDBS
Liu^{70} (2009)	$\mathrm{Fe_3O_4}$	sodium citrate	sodium acetate	EG	200	hydrothermal	varying cluster diameter 80–410 nm	amount of iron precursor and ligand
Liu^{71} (2017)	$\mathrm{ZnFe_2O_4}$	N/A	sodium acetate	EG	200	hydrothermal	Varying cluster diameter 330–560 nm	amount of sodium acetate
Lu^{72} (2016)	$\mathrm{Fe_3O_4}$	PEG diacid (Mn = 600 Da) and oleate	N/A	phenyl ether	260	thermal decom- position	cluster diameter at 25 and 62 nm	amount of iron precursor and ligand
Luo^{73} (2009)	$\mathrm{Fe_3O_4}$	N/A	sodium acetate	EG	200	hydrothermal	varying cluster diameter 90–260 nm	reaction time
Pereira ⁷⁴ (2015)	Fe ₃ O ₄ /Fe ₂ O ₃ mixed phase	alkanolamines diethanolamine (DEA), triethanolamine (TEA) and triisopropanolamine (TIPA)	N/A	hydrochloric acid	100	thermal decomposition	varying cluster diameter (DLS) 30–40 nm	using different ligand

Table 1. continued

reference	composition	capping agent	alkaline	solvent	reaction temp $(^{\circ}C)$	reaction temp ($^{\circ}$ C) reaction method	size range	size control
$Togashi^{60} \left(2011\right) Fe_3O_4$	Fe_3O_4	3,4-dihydroxyhydroxycinnamic acid (DHCA 98%)	potassium hydrorxide	water	250	250 hydrothermal	varying cluster diameter 50–400 nm	reaction time
Tong ⁷⁵ (2015)	Fe_3O_4/Fe_2O_3 mixed phase	PEG-2000	sodium carbo- nate	EG	200	hydrothermal	varying cluster diameter 30–290 nm	amount of water
Wang ⁴⁹ (2006)	Fe_3O_4	1,6-hexanediamine	sodium acetate	EG	190–205	hydrothermal	varying cluster diameter 100–200 nm	amount of iron precursor
Wang ⁷⁶ (2013)	Fe_3O_4	poly(diallyldimethylammonium chloride) (PDDA)	sodium acetate	EG	200	hydrothermal	varying cluster diameter 90–350 nm, varying nanocrystal size 15–35 nm	amount of PDDA
Wang ⁷⁷ (2015) Fe ₃ O ₄	Fe_3O_4	sodium citrate	sodium acetate	EG and DEG	200	200 hydrothermal	varying cluster diameter 60–250 nm, varying nanocrystal size 6–9 nm	ratio of solvent
Wei ⁵⁹ (2018)	Fe_3O_4	PAA	sodium hydrox- ide	DEG	200	thermal decom- position	varying cluster diameter 15–70 amount of PAA nm	amount of PAA
Xi ⁴⁶ (2008)	Fe_3O_4	Oleic acid	sodium acetate	EG	200	hydrothermal	varying cluster diameter 100–400 nm	amount of iron precursor
$ Kim^{78} (2019) $	Fe_3O_4 and $Mn_xFe_{3-x}O_4$	N/A	sodium acetate	EG	200	200 thermal decomposition	cluster diameter 29 and 33 nm using different metal precursor	using different metal precursor

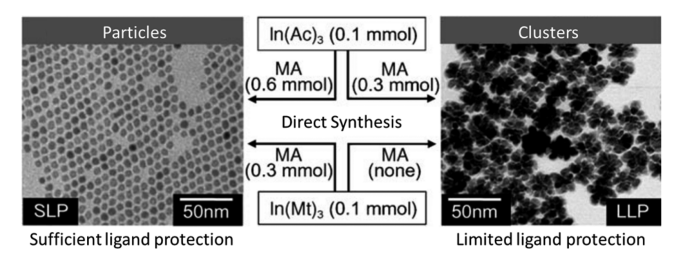


Figure 2. The formation of nanocrystal clusters, because of the limited ligand protection (LLP). Under sufficient ligand protection (SLP), isolated nanocrystals were formed. In LLP, particles had a tendency to form clusters to minimize the surface energy. [Figure adapted from ref 51 with permission. Copyright 2006, John Wiley and Sons.]

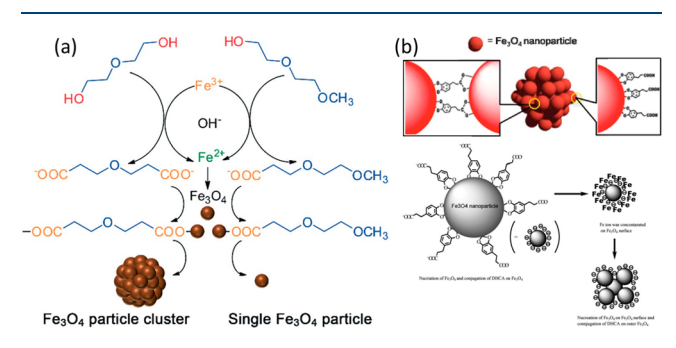


Figure 3. Schematic illustration of the cluster formation due to the conjugative molecules in the reaction. (a) The primary nanocrystals were interconnected by dicarboxylic acids. [Figure adapted from ref 60 with permission. Copyright 2011, Royal Society of Chemistry, London.] (b) The primary nanocrystals were interconnected by 3,4-dihydroxyhydroxycinnamic acid (DHCA). [Figure adapted from ref 59 with permission. Copyright 2018, Royal Society of Chemistry, London.]

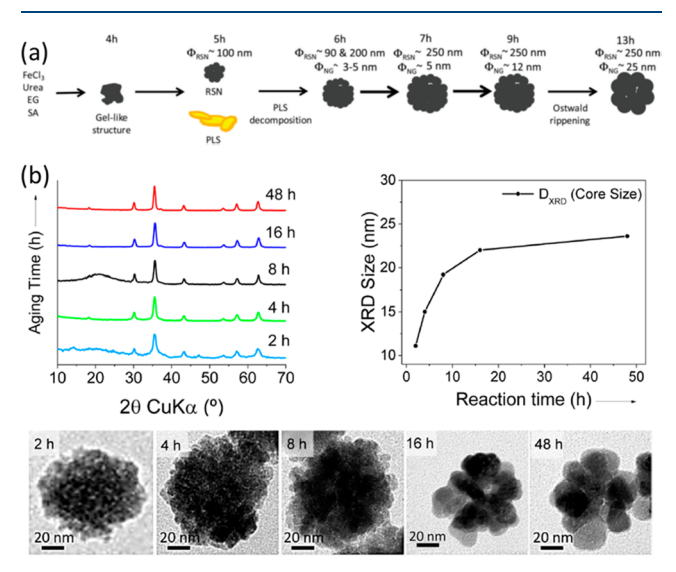


Figure 4. The effect of Ostwald ripening on the morphology of the clusters. (a) Schematic illustration of the formation of the clusters. Figure adapted from ref 57 with permission. Copyright 2017 Royal Society of Chemistry. (b) Time-dependent observation on the formation of the nanoclusters corresponding to the Ostwald ripening. Both TEM and XRD showed the nanocrystals with increasing size over time. [Figures adapted from ref 58 with permission. Copyright 2017 American Chemical Society, Washington, DC.]

and aggregation has not been well-established. The reaction system and conditions for dimension control were usually determined through extensive experimentation. Researchers have developed many procedures to generate magnetic nanocrystal clusters with different dimensions. The reaction schemes used are summarized in Table 1.

III.1. Concentration of the Reactants. The hydrolysis rate of metal precursors plays a vital role in controlling the size of clusters. It was found that the hydrolysis rate of the precursors is positively correlated to the cluster size. Ge et al. prepared magnetite clusters from 30 to 180 nm by simply changing sodium hydroxide concentration. 45 Hydroxide in the solution can create an alkaline medium that induces the forced hydrolysis of iron precursors at high temperatures. The increase of sodium hydroxide concentration accelerated the hydrolysis rate, thus leading to a high concentration of primary particles. The high concentration of primary particles might result in a larger cluster diameter. Their flexible synthesis with an accurate size control on the clusters was a milestone for discovering the size-dependent properties of the clusters. The hydrolysis rate can also be increased by increasing the amount of metal precursors. Liu et al. synthesized clusters from 80 nm to 400 nm by simply increasing the concentration of iron chloride from 0.05 to 0.25 mmol L⁻¹.⁷⁰

The ratio between the ligand and the metal precursor significantly influences the cluster size. Several studies found that the ligand:metal precursor ratio is negatively correlated to the cluster size. Cheng et al. found that the size of the magnetite clusters decreased when concentration of the ligand, sodium citrate was increased. This finding is in agreement with the LLP mechanism. The authors synthesized uniform magnetite clusters by changing the concentration of the ligands (Figure 5). As the ratio of ligand to precursor increased from 1/120 to 100/120, the cluster diameter decreased from 300 to 40 nm. Part of the carboxylic groups on the citrate form the dative bond with the iron oxide core, while the rest can provide electrostatic stabilization against other clusters. Using

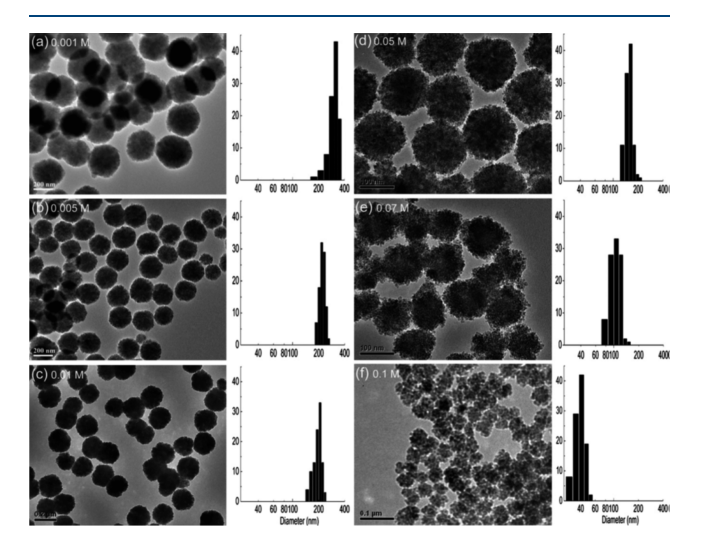


Figure 5. The effect of the ligand concentration on the cluster size. The clusters with decreasing cluster diameter from 300 to 40 nm by increasing sodium citrate concentration in the synthesis. The clusters have good uniformity, and the standard deviation of the cluster diameter measured by TEM is <20%. [Figure adapted from ref 48 with permission. Copyright 2009, Royal Society of Chemistry, London].

another reaction system, Wei et al. successfully controlled the cluster diameter from 15 nm to 70 nm by reducing the amount of poly(acrylic acid) (PAA) from 8 mmol to $0.^{59}$ The clusters prepared without PAA were coated with the dicarboxylic acids that originated from the solvent ethylene glycol. In addition to the concentration of the ligands, the ligand:metal precursor ratio can also be varied by changing the concentration of the metal precursor, thus generating clusters of different sizes. 49,70,72

III.2. Pretreatment of the Reaction Mixture. The pretreatment of the reaction mixture also affects the size of clusters. Lin et al. prepared magnetite clusters of different sizes by sonicating the reaction mixture for different periods of time (Figure 6). They found that longer sonication pretreatment

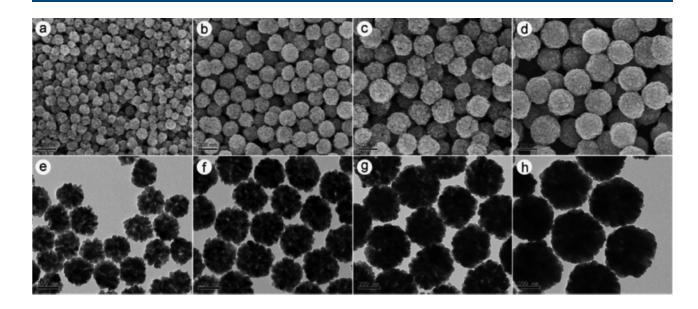


Figure 6. The effect of the sonication pretreatment on the morphology of clusters. (a–d) SEM and (e–h) TEM images of four cluster samples obtained from different times of sonication pretreatment: (a, e) 40 min, (b, f) 30 min, (c, g) 15 min, and 5 min (d, h), while other parameters were kept unchanged (0.68 g of FeCl $_3$ · 6H $_2$ O, 1.2 g of NaAc, and 0.034 g of EDTA-2Na in 20 mL of ethylene glycol at 200 °C for 10 h). Figure adapted from ref 62 with permission. Copyright 2013 American Chemical Society.

on the reaction mixture led to small clusters. This is because the precursors and the ligands were more readily combined to form the primary nanocrystals when the sonication time was longer. Although such a method is simple and effective, the mixing effect is difficult to quantify. This method may not be well-reproducible. This study suggests that the reactants should be well-mixed in the solvent before increasing temperature to achieve good control over the cluster size in the reaction.

III.3. Solvent. Another factor that influences the size of clusters is the selection of solvent. The polyol solvent also serves as a reducing agent in generating the magnetite nanocrystal clusters. After going through forced hydrolysis, the iron(III) salt will form Fe(OH)₃ that is partially subject to reduction by the polyols to form Fe(OH)₂ and convert to Fe₃O₄ eventually.⁷⁹ The reducing capacity of the polyols determines the rate of the formation of the monomers, thus changing the size of the clusters. Different types of polyols have been used to tune the cluster size.⁴⁷ Using a mixture of two polyols as solvent provides an efficient way to vary the reducing capacity of the solvent. Huang et al. reported the synthesis of magnetite clusters from 50 to 400 nm by changing the ratio of ethylene glycol to diethylene glycol.⁶⁸ With the increase of the diethylene glycol content, the clusters formed in such solvent mixture became smaller. No clusters were formed in a pure diethylene glycol solvent, which could be ascribed to the extremely slow reduction that impeded the growth of the clusters. Similar observations have been reported using other polyols, such as triethylene glycol, 1,2-propanediol, and polyethylene glycol.

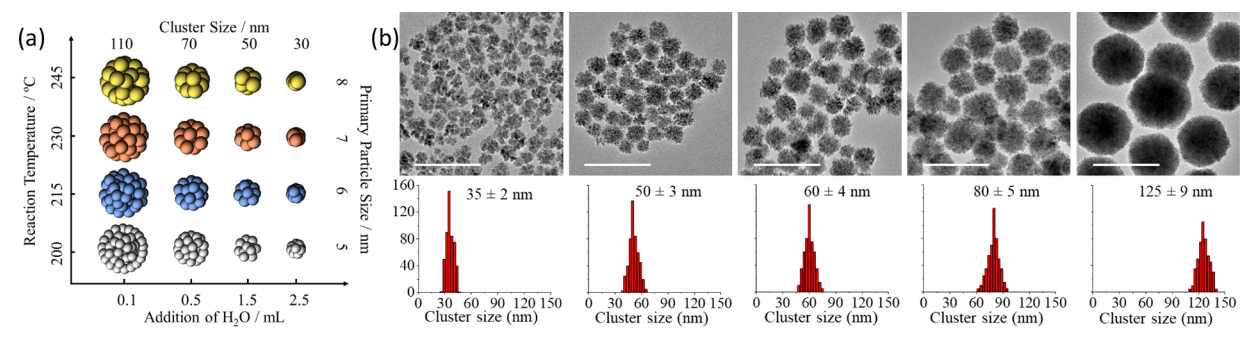


Figure 7. Synthesis of clusters with independent control of cluster size and primary particle size. (a) Proposed scheme for the independent dimensional control of the clusters. The amount of water can only dictate the cluster size, while the reaction temperature can determine the primary nanocrystal size. A library of clusters, with the cluster diameter of 20–200 nm and the size of the primary nanocrystals of 4–10 nm, can be formed in this synthetic system. (b) TEM images and size distributions of the cluster samples with different cluster sizes. Scale bar = 200 nm. The amount of added water for each cluster sample synthesis, from left to right, was 2.0, 1.5, 1.0, 0.4, and 0.1 mL. [Figure adapted from ref 80 with permission. Copyright 2020, American Chemical Society, Washington, DC.]

III.4. Addition of Water. The addition of a small amount of water into the reaction mixture could dramatically reduce the size of clusters. The addition of water to the solvent will cause the reduction of the viscosity, thus leading to smaller clusters. The viscosity of water is ~1 mPa s at room temperature, whereas the typical value for various glycols is ~15–30 times higher. In a highly viscous medium, the movement of the primary nanocrystals is more kinetically confined and has a tendency to form larger clusters. Conversely, when the primary nanocrystals have higher mobility in a less-viscous medium, smaller clusters can be formed. Hemery et al. found that the diameter of the maghemite clusters decreased from 50 nmto 16 nm by increasing the amount of water in the solvent.

III.5. Independent Control of Cluster Size and Primary Particle Size. By varying two or more factors, it is possible to control both the cluster size and nanocrystal size. Xiao et al. successfully developed libraries of clusters with independent dimensional control over the two parameters by changing the amount of water and the reaction temperature (Figure 7).80 In this work, iron chloride, poly(acrylic acid), urea, and ethylene glycol were used as the iron precursor, the stabilizing agent, the base, and the solvent, respectively. In this reaction system, the amount of water only affected the size of the cluster and had a negligible effect on the primary nanocrystal size. The reaction temperature only influenced the primary nanocrystal size and had a negligible effect on the cluster size. Changing the reaction temperature and amount of water provides an efficient approach to produce the magnetite nanocrystal cluster library with tunable cluster size and primary particle size. Change of other reaction conditions, such as the concentration of ligands (polyacrylate) and iron precursors, can affect the sizes of both clusters and primary particles. Nevertheless, this method was only applicable when urea was used to provide the alkaline environment for forced hydrolysis of the iron precursors. In some other reaction systems where sodium acetate was used as a base, change in the cluster size was usually accompanied by the change of the primary nanocrystal size, and vice versa, as reported by Xuan et al. This was ascribed to the fact that the acetate also binds to the nanocrystal surface.48

III.6. Ferrite Clusters. While most strategies to control the cluster dimensions were exploited using magnetite as an example, these strategies can be used in other metal oxide systems such as maghemite and ferrites. Liu et al. synthesized

zinc ferrite $(ZnFe_2O_4)$ clusters with a size range of 300-600 nm. They found that increase in the concentration of sodium acetate led to a reduction of cluster size. A library of ferrite clusters, including manganese, cobalt, and nickel, have been reported by Otero-Lorenzo et al. These materials greatly expand the library of magnetic nanocrystal clusters and provide a rich source for scientific exploration and technological development.

IV. PROPERTIES AND APPLICATIONS OF MAGNETIC NANOCRYSTAL CLUSTERS

IV.1. Magnetic Properties of Clusters. The magnetic nanocrystal clusters display unique magnetic properties that are different from their constituent primary particles because of the unique structure of the clusters. These magnetic properties arise from the interactions between primary nanocrystals within the cluster. Particularly, the clusters might show more attractive properties when the primary particles within a cluster assume the same crystallographic orientation (Figure 8). One interesting property is that the clusters may remain

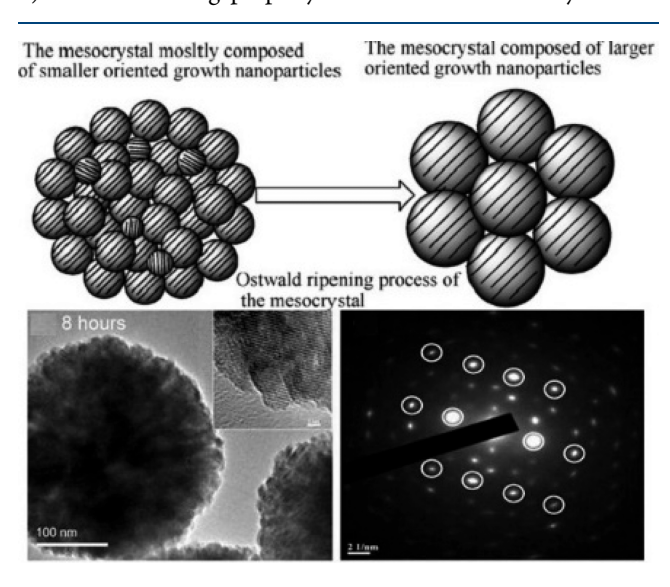


Figure 8. Oriented attachment of the primary nanocrystals. The parallel orientation of the primary nanocrystals was facilitated by Ostwald ripening. [Figure adapted from ref 47 with permission. Copyright 2011, Royal Society of Chemistry, London.]

superparamagnetic for hundreds of nanometers. These superparamagnetic clusters assume much more magnetic volume than the isolated nanocrystals. 44,45,80 In addition, magnetic nanocrystal clusters show high saturation magnetization (see Figure 9). These unique properties are not only interesting

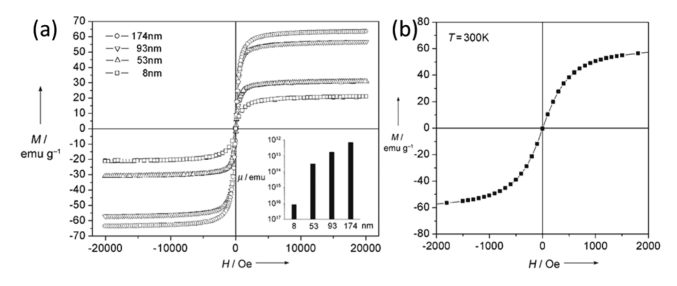


Figure 9. Magnetic properties of clusters. (a) The magnetization curves of the clusters with different sizes. (b) The 93-nm clusters demonstrated superparamagnetic behavior with zero coercivity and remanence at room temperature. [Figure adapted from ref 45 with permission. Copyright 2007, John Wiley and Sons.]

for fundamental research but also useful for technological development, since these properties make the clusters more efficient for moving, heating, and imaging in many applications. The application of these materials in many different fields has been explored.

IV.2. Biomedical Applications. Another interesting feature of magnetic nanocrystal clusters is their high uptake by various types of cells. Hemery et al. studied the uptake of 30 nm clusters coated with polyethylene glycol (PEG) using U87 gliobnlastoma cells.⁸⁵ Both the confocal and TEM images show that the clusters were localized in the lysosomes of the cells, suggesting the clusters were uptaken through an endocytosis pathway (see Figure 10). The number of clusters entering the cell was much higher than the isolated iron oxide nanocrystals. Kim et al. investigated the uptake of magnetite and manganese ferrite clusters using a vibrating-sample magnetometer.⁷⁸ After incubating the cancer cells with the clusters, internalization of the clusters was determined by measuring the magnetization of the cells. They found that the uptake of the clusters was dependent on the type of cells. MCF10A cells had the highest cellular uptake capability among various types of cells. The authors also found the roughness of the cluster surface had significant impact on the cellular uptake, where the clusters covered with protein corona were preferably taken up by the cells. The clusters remain their morphology in all the in vivo applications, since they are hard aggregates. While large clusters show higher delivery efficiency in the in vitro studies, more work are needed to determine the optimal size for the in vivo applications, since large clusters will be cleared by the mononuclear phagocytic system.

The magnetic clusters are very efficient in generating heat under the alternating magnetic field (AMF), which makes them a good candidate for hyperthermia cancer treatment. Lartigue et al. prepared the maghemite clusters and compared their magnetic heating performance with isolated nanocrystals. They found that clusters outperformed isolated nanocrystals. When placed in the same AMF, the clusters could elevate the temperature of the surrounding solution up to 35 $^{\circ}$ C within \sim 30 s, which was seven times greater than that of conventional nanocrystals at the same concentration (see Figure 11a). They attributed the improved performance of clusters to the cooperative magnetic behavior of primary particles within a

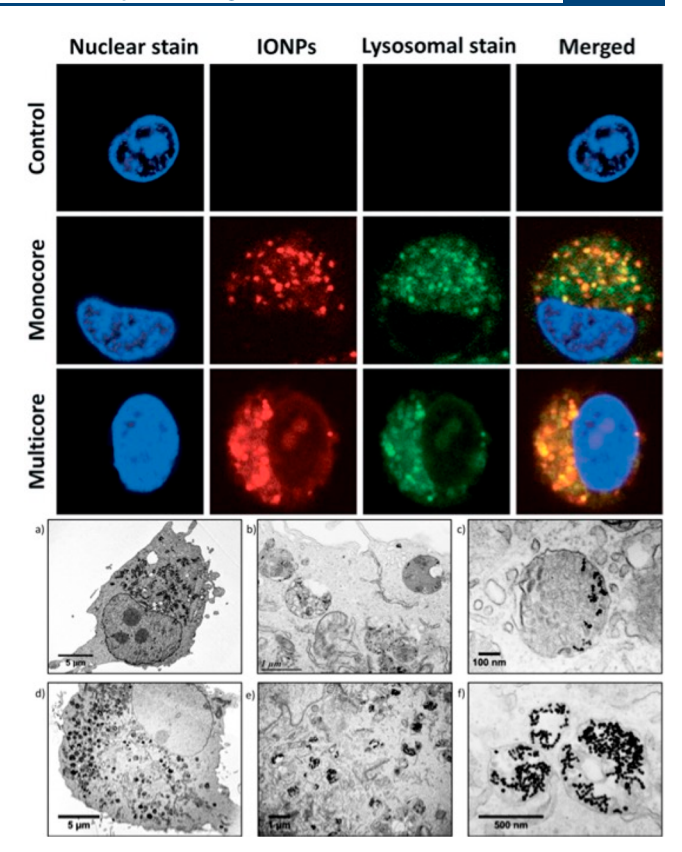


Figure 10. Cellular localization of clusters. The confocal and TEM images showing the localization of clusters (multicore) and particles (monocore) in cells. U87 glioblastoma cells were incubated with 15 nm nanocrystals and 30 nm clusters to load the nanocrystals. [Figure adapted from ref 85 with permission. Copyright 2017, Royal Society of Chemistry, London.]

cluster. The enhanced magnetic heating of clusters was also reported by Hemery et al. 63 They found that the magnetic heating performance of clusters increases with the cluster diameter in the range of 10–35 nm (see Figure 11b). The improved magnetic heating performance of clusters was used to kill tumor cells by Lartigue et al. 44 The MCF-7 tumor cells were incubated with the 24 nm clusters to load the clusters into the cells. The TEM images show the clusters were localized in the lysosomes of the cells (see Figure 12). A cluster loading of 8 pg per cell could be achieved using the clusters with an iron concentration of 2 mM. When the cells loaded with clusters were placed in an AMF with a field strength of 29 kA/m and a frequency of 520 kHz, the temperature of the cells increased to 50 °C, leading to a cell death rate of 60%.

Clusters have also been used as the magnetic resonance imaging (MRI) contrast agent and showed excellent performance. Maity et al. compared the properties and performance of 44 nm magnetite clusters with 10 nm isolated nanocrystals (Figure 13). They found that the clusters display both much higher specific absorption rate (SAR) value and higher T2 relaxivity for MRI, making the clusters an ideal multifunctional platform for both treatment and imaging. In their *in vivo* experiments, the clusters were injected into mice with subcutaneous xenograft tumors of MCF-7 cancer cells. The MRI images show that the intensities in the kidney and the liver were enhanced, which was due to the clearance of the clusters by these organs. However, the intensities decayed over time, and the post-contrast of these sites was not obvious. In

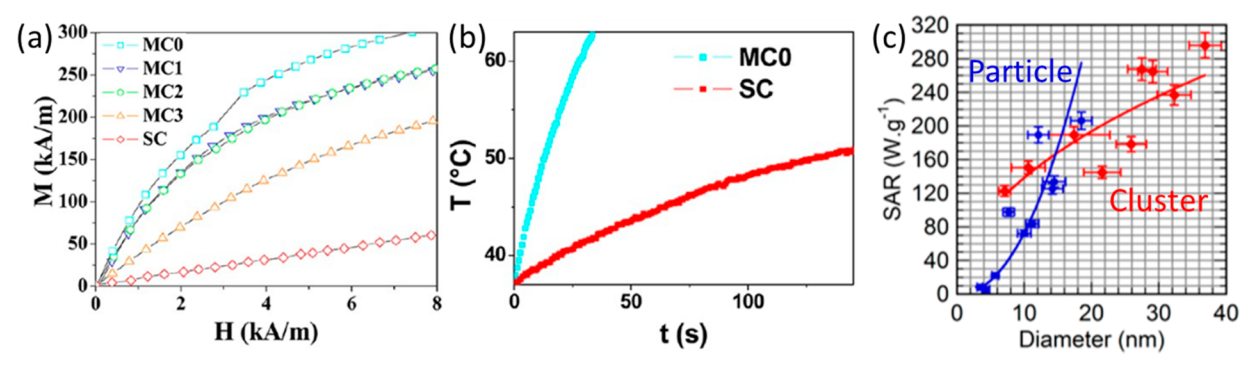


Figure 11. Superior magnetic heating efficiency of iron oxide nanocrystal clusters. (a) The low field magnetization and (b) the heating of the clusters and the particles. [Figures adapted from ref 44 with permission. Copyright 2012, American Chemical Society, Washington, DC.] (c) The SAR of the clusters and particles with different sizes. The clusters outperformed the particles in nearly all size ranges in both cases. [Figure adapted from ref 63 with permission. Copyright 2017, American Chemical Society, Washington, DC.]

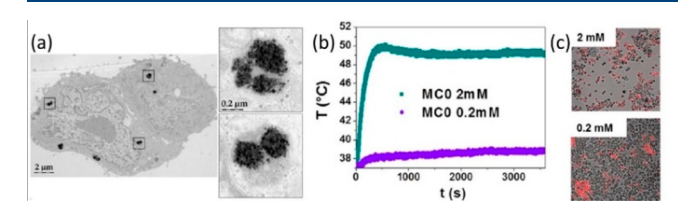


Figure 12. The application of clusters as heating mediator for magnetic hyperthermia *in vitro*. (a) The TEM images of the MCF-7 tumor cells containing the clusters. (b) The magnetic heating of the cells treated with 2 mM and 0.2 mM clusters in the AMF. (c) The death assessment of the cells placed in the AMF. [Figure adapted from ref 44 with permission. Copyright 2012, American Chemical Society, Washington, DC.]

(a)	Avaraga		Relaxivity/s ⁻¹ mM ⁻¹	
Samples	Average particle size/nm	$M_{\rm s}$ /emu g ⁻¹	r2	r2*
MNC-10	10	63	205.6	309.2
MNC-14	44	75	294.99	450.05

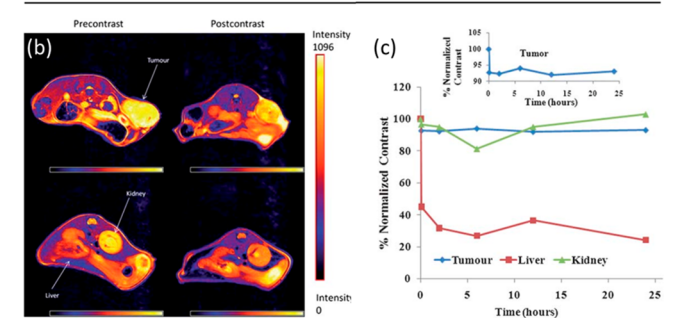


Figure 13. The application of clusters as MRI contrast agent *in vivo*. (a) The relaxivities of the isolated nanocrystals and clusters. Sample MNC-10 and MNC-14 were 10 nm nanocrystals and 44 nm clusters, respectively. (b) The MRI image of the SCID mice using clusters as a contrast agent. (c) The MRI signals in the tumor sites remained nearly the same over 25 h. [Figure adapted from ref 65 with permission. Copyright 2011, Royal Society of Chemistry, London.]

contrast, the clusters retained in the tumor much longer and the signals from the tumor nearly remained the same over the entire operation. This was ascribed to the enhanced permeation and retention mechanism where the clusters passively targeted the tumor sites by penetrating through the leaky vasculature of the tumor.

Magnetic nanocrystal clusters can serve as a multifunctional nanoplatform for disease treatment. Wang et al. designed a nanoplatform composed of iron oxide clusters and polypyrrole (PPy) for remotely controlled cancer therapy. (See Figure 14. 86) Poly(ethylene glycol) was coated on the surface of the

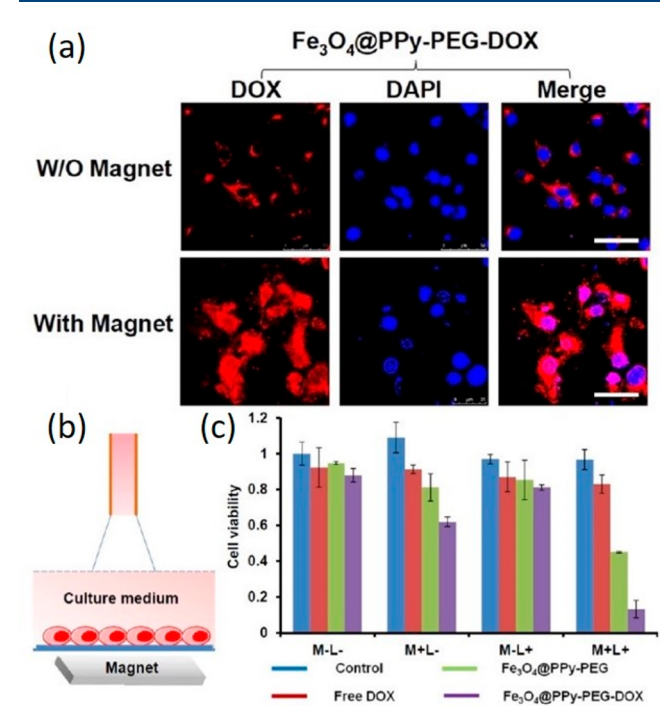


Figure 14. The application of clusters as a multifunctional platform for improved drug delivery. (a) Confocal images of 4T1 cells incubated with Fe₃O₄@PPy-PEG-DOX. (b) Schematic illustration of *in vitro* combined therapy. (c) Relative viabilities of 4T1 cells after different treatment. [Figure adapted from ref 86 with permission. Copyright 2013, American Chemical Society, Washington, DC.]

platform to improve its biocompatibility and stability. The iron oxide nanocluster was used for both magnetically controlled drug delivery and T2-weighted MRI. The PPy not only serves as a photothermal agent but also was used for drug loading and release. It allows the clusters to release doxorubicin when irradiated by near-infrared light. Moreover, the cancer cells containing the clusters were captured by magnets and could increase the selectivity of the near-infrared irradiation. The *in vitro* experiment showed that the cell viability was <0.15 with the external field, whereas the clusters were nearly harmless to the cells in the control experiment. In the *in vivo* studies, the

tumor growth in the mice was clearly inhibited when applying this nanoplatform.

IV.3. Environmental Applications. The application of magnetic clusters in environmental remediation has also been explored. Because of the unique structure and magnetic properties of clusters, they are ideal materials to capture pollutants and toxic composites from wastewater. Because of the porous structure of the clusters, they have more specific surface areas than the isolated nanocrystals with similar overall sizes, which give rise to high absorption capacity. The big magnetic moment of clusters makes them easy to be captured by a magnet. Wang et al. synthesized the magnetite clusters with an average size of 95-350 nm and studied their performance in removing arsenic pollutants.⁷⁶ The clusters were coated with a positively charged polymer, poly-(diallyldimethylammonium chloride), to increase their affinity toward the As(III) and As(V) species, which are negatively charged. They found that, in both experiments for removal, the clusters showed high capacities for the adsorption of the As(III) and As(V). The adsorption capacity depends on the cluster size. The clusters with an average size of 200 nm had the best efficiency for low-level arsenic removal, because of their larger magnetization and better colloidal stability (Figure 15a). In another paper from the same group, the authors used

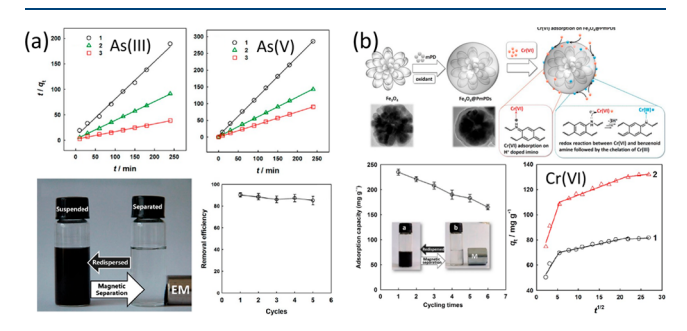


Figure 15. Clusters for toxic metal removal. (a) The adsorption of As(III) and As(V) using magnetite clusters. The clusters were coated with poly(diallyldimethylammonium chloride) (PDDA). The sizes for 1, 2, and 3 were 215, 195, and 185 nm, respectively. The adsorption of both As(III) and As(V) followed the pseudo-second-order rate kinetic model, where the equilibrium adsorption capacity was inversely proportional to the slope of the curve. The 185 nm clusters had the highest adsorption performances. [Figure adapted from ref 76 with permission. Copyright 2013, American Chemical Society, Washington, DC.] (b) The adsorption of Cr(VI) using magnetite clusters coated with poly(m-phenylenediamine) (PmPDs). The cluster diameter was ~200 nm, and the coating thickness was ~50 nm. [Figure adapted from ref 87 with permission. Copyright 2015, American Chemical Society, Washington, DC.]

clusters coated with poly(*m*-phenylenediamine) to remove Cr(VI) species in the water. Poly(*m*-phenylenediamine can reduce Cr(VI) to Cr(III) and then chelate to Cr(III) species for better adsorption (Figure 15b).⁸⁷ Both studies showed high removal efficiency of the toxic metal from wastewater and satisfactory durability where the clusters can be recycled more than five times with little decrease in performance.

IV.4. Photonic Applications. Another interesting application of the superparamagnetic clusters is as photonic crystal. Magnetic nanocrystal clusters can form responsive photonic crystals in an external field. Xia et al. synthesized 100–200 nm clusters and observed a clear colored pattern of the aqueous solution when placed on a magnet (Figure 16a). The color of

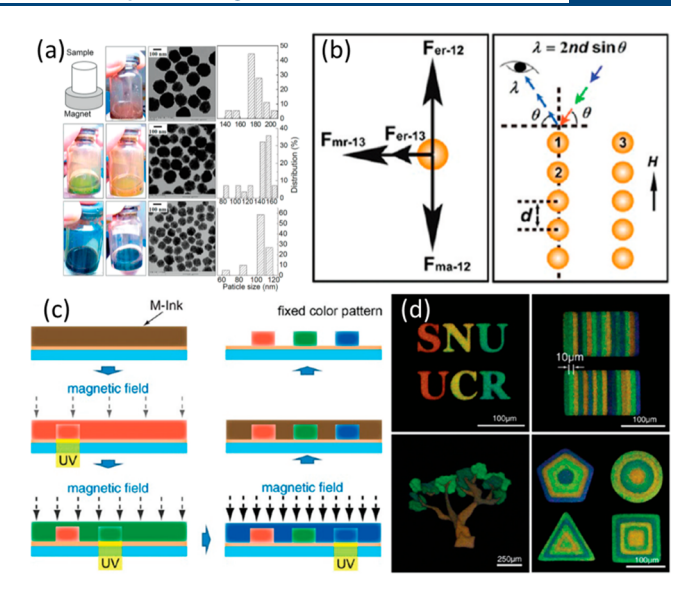


Figure 16. Clusters for reversible photonic crystal with magnetically controllable bandgap. (a) The optical images of the clusters placed in a static magnetic field and the TEM images of the clusters with their size distribution. [Figure adapted from ref 88 with permission. Copyright 2009, American Chemical Society, Washington, DC.] (b) Illustration of the clusters forming photonic crystals. (c) Applying clusters for structural color printing. [Figures in panels (b) and (c) were adapted from ref 89 with permission. Copyright 2012, American Chemical Society, Washington, DC.] (d) Picture of the high-resolution printing using photonic crystals. [Figure adapted from ref 90 with permission. Copyright 2009, Springer Nature.]

the solution was dependent on the cluster size, where smaller clusters exhibited a purple color while larger ones became brown to red. He et al. attributed this color change to the Bragg diffraction of the cluster chains (Figure 16b). ⁸⁹ The clusters form chains along the direction of the field in a static magnetic field because of the balance between the attractive magnetic dipolar force and the repulsive steric or electrostatic force of the clusters. The distance between clusters in the chain is influenced by the size and coating of the cluster as well as the magnetic field strength. ⁶⁹ When this distance is within the optical wavelength range, the light with a specific wavelength can be reflected due to Bragg diffraction, therefore presenting the unique color of the cluster solution.

The magnetic nanocrystal clusters have been applied to color production since the bandgap of the photonic crystal can be controlled by varying the strength of the magnetic field. Kim et al. proposed structural color printing using the clusters (Figure 16c). 90,91 The authors invented a material called Mink, which was composed of magnetic nanocrystal clusters, solvation liquid, and photocurable resin. The external field was used to reversibly control the color of the photonic crystal. When exposed to UV light, the photocurable resin would polymerize and fix the colored pattern of the clusters in the field. The sequential steps of "tuning and fixing" finally lead to multicolor printing with high resolution and quality. This proposed structural color printing scheme significantly impacted color production, since it may replace conventional dyes that cause severe environmental pollution.

V. CONCLUSIONS AND OUTLOOK

In this Review, we have examined the recent advances in the synthesis and applications of magnetic nanocrystal clusters.

Solution chemistry has been demonstrated to be an efficient method to synthesize clusters with controlled dimensions. The clusters might be formed through different mechanisms in various reaction systems such as limited ligand protection, ligand cross-linking, and so on. The size of clusters and primary particles can be varied by selecting different reactants and changing reaction conditions. A large library of clusters with different compositions, cluster sizes, and primary particle sizes has been generated. Compared to the conventional isolated nanocrystals, the clusters exhibit superior magnetic properties, because of the intracluster interactions. The superior magnetic properties of clusters make them useful in various industrial and biomedical applications.

While magnetic nanocrystal clusters are promising for many applications, there are still substantial challenges to address before making full use of these interesting materials. The physics underlying their interesting magnetic properties have not been well understood. Micromagnetics simulation will provide a powerful tool to understand the physics and predict the dependence of the magnetic properties on the cluster size and primary particle size. Although many methods have been reported to synthesize clusters, the reproducibility and scalability of these synthesis methods remain a challenge due to the lack of understanding of the formation process of clusters. More mechanistic studies are needed to elucidate this complicated process. Another challenge for applying clusters is to improve the colloidal stability of clusters in various media. Most cluster samples synthesized using current methods are only stable in pure water, and they tend to aggregate in many biological and environmental media, limiting their extensive applications. 47,49,67,80,92 New surface coating chemistry is needed to stabilize the clusters in various media. The safety of the clusters must be evaluated before applying these materials in a clinical setting. 93-97 With the excellent magnetic properties, magnetic nanocrystal clusters are expected to find applications in many fields such as magnetic particle imaging, biosensing, etc. 98-103

■ AUTHOR INFORMATION

Corresponding Authors

Qingbo Zhang – Department of Bioengineering, Rice University, Houston, Texas 77005, United States;

orcid.org/0000-0001-8289-0227;

Email: qingbo.zhang@rice.edu

Gang Bao – Department of Bioengineering, Rice University, Houston, Texas 77005, United States; ⊚ orcid.org/0000-0001-5501-554X; Email: gang.bao@rice.edu

Authors

Zhen Xiao – Department of Chemistry, Brown University, Providence, Rhode Island 02912, United States;

orcid.org/0000-0002-3740-3546

Linlin Zhang — Department of Bioengineering, Rice University, Houston, Texas 77005, United States; ⊙ orcid.org/0000-0003-3240-1215

Vicki L. Colvin – Department of Chemistry, Brown University, Providence, Rhode Island 02912, United States;

orcid.org/0000-0002-8526-515X

Complete contact information is available at: https://pubs.acs.org/10.1021/acs.iecr.1c04879

Notes

The authors declare no competing financial interest.

ACKNOWLEDGMENTS

This work was supported in part by the National Institutes of Health (No. UG3HL151545 to G.B.).

ABBREVIATIONS

LLP = limited ligand protection

SLP = sufficient ligand protection

TEG = triethylene glycol

TTEG = tetraethylene glycol

DHCA = 3,4-dihydroxyhydroxycinnamic acid

TEM = transmission electron microscopy

HRTEM = high-resolution TEM

XRD = X-ray diffraction

SAED = selected area electron diffraction

PEG = polyethylene glycol

AMF = alternating magnetic field

SAR = specific absorption rate

MRI = magnetic resonance imaging

UV = ultraviolet

MPI = magnetic particle imaging

REFERENCES

- (1) Bean, C.; Livingston, u. D. Superparamagnetism. *J. Appl. Phys.* **1959**, 30 (4), S120–S129.
- (2) Knobel, M.; Nunes, W.; Socolovsky, L.; De Biasi, E.; Vargas, J.; Denardin, J. Superparamagnetism and other magnetic features in granular materials: a review on ideal and real systems. *J. Nanosci. Nanotechnol.* **2008**, *8* (6), 2836–2857.
- (3) Mikhaylova, M.; Kim, D. K.; Bobrysheva, N.; Osmolowsky, M.; Semenov, V.; Tsakalakos, T.; Muhammed, M. Superparamagnetism of magnetite nanoparticles: dependence on surface modification. *Langmuir* **2004**, 20 (6), 2472–2477.
- (4) Cardoso, V. F.; Francesko, A.; Ribeiro, C.; Bañobre-López, M.; Martins, P.; Lanceros-Mendez, S. Advances in magnetic nanoparticles for biomedical applications. *Adv. Healthcare Mater.* **2018**, 7 (5), 1700845.
- (5) Mohammed, L.; Gomaa, H. G.; Ragab, D.; Zhu, J. Magnetic nanoparticles for environmental and biomedical applications: A review. *Particuology* **2017**, *30*, 1–14.
- (6) Mou, X.; Ali, Z.; Li, S.; He, N. Applications of magnetic nanoparticles in targeted drug delivery system. *J. Nanosci. Nanotechnol.* **2015**, *15* (1), 54–62.
- (7) Vaghari, H.; Jafarizadeh-Malmiri, H.; Mohammadlou, M.; Berenjian, A.; Anarjan, N.; Jafari, N.; Nasiri, S. Application of magnetic nanoparticles in smart enzyme immobilization. *Biotechnology letters* **2016**, 38 (2), 223–233.
- (8) Zhou, Z.; Yang, L.; Gao, J.; Chen, X. Structure-relaxivity relationships of magnetic nanoparticles for magnetic resonance imaging. *Adv. Mater.* **2019**, *31* (8), 1804567.
- (9) Wei, H.; Bruns, O. T.; Kaul, M. G.; Hansen, E. C.; Barch, M.; Wiśniowska, A.; Chen, O.; Chen, Y.; Li, N.; Okada, S.; et al. Exceedingly small iron oxide nanoparticles as positive MRI contrast agents. *Proc. Natl. Acad. Sci. U. S. A.* **2017**, *114* (9), 2325–2330.
- (10) Li, Q.; Kartikowati, C. W.; Horie, S.; Ogi, T.; Iwaki, T.; Okuyama, K., Correlation between particle size/domain structure and magnetic properties of highly crystalline Fe3O4 nanoparticles *Sci. Rep.* **2017**, 7. DOI: 10.1038/s41598-017-09897-5
- (11) Mohapatra, J.; Zeng, F. H.; Elkins, K.; Xing, M. Y.; Ghimire, M.; Yoon, S.; Mishra, S. R.; Liu, J. P. Size-dependent magnetic and inductive heating properties of Fe3O4 nanoparticles: scaling laws across the superparamagnetic size. *Phys. Chem. Chem. Phys.* **2018**, 20 (18), 12879–12887.
- (12) Patsula, V.; Moskvin, M.; Dutz, S.; Horak, D. Size-dependent magnetic properties of iron oxide nanoparticles. *J. Phys. Chem. Solids* **2016**, *88*, 24–30.

- (13) Yoo, K.; Jeon, B. G.; Chun, S. H.; Patil, D. R.; Lim, Y. J.; Noh, S. H.; Gil, J.; Cheon, J.; Kim, K. H. Quantitative Measurements of Size-Dependent Magnetoelectric Coupling in Fe3O4 Nanoparticles. *Nano Lett.* **2016**, *16* (12), 7408–7413.
- (14) Wu, L.; Mendoza-Garcia, A.; Li, Q.; Sun, S. Organic phase syntheses of magnetic nanoparticles and their applications. *Chem. Rev.* **2016**, *116* (18), 10473–10512.
- (15) Kudr, J.; Haddad, Y.; Richtera, L.; Heger, Z.; Cernak, M.; Adam, V.; Zitka, O. Magnetic nanoparticles: From design and synthesis to real world applications. *Nanomaterials* **2017**, *7* (9), 243.
- (16) Majidi, S.; Zeinali Sehrig, F.; Farkhani, S. M.; Soleymani Goloujeh, M.; Akbarzadeh, A. Current methods for synthesis of magnetic nanoparticles. *Artificial cells, nanomedicine, and biotechnology* **2016**, 44 (2), 722–734.
- (17) Sun, S.; Zeng, H. Size-controlled synthesis of magnetite nanoparticles. J. Am. Chem. Soc. 2002, 124 (28), 8204–8205.
- (18) Lisjak, D.; Mertelj, A. Anisotropic magnetic nanoparticles: A review of their properties, syntheses and potential applications. *Prog. Mater. Sci.* **2018**, *95*, 286–328.
- (19) Obaidat, I. M.; Issa, B.; Haik, Y. Magnetic properties of magnetic nanoparticles for efficient hyperthermia. *Nanomaterials* **2015**, 5 (1), 63–89.
- (20) Caruntu, D.; Caruntu, G.; O'Connor, C. J. Magnetic properties of variable-sized Fe3O4 nanoparticles synthesized from non-aqueous homogeneous solutions of polyols. *J. Phys. D: Appl. Phys.* **2007**, *40* (19), 5801–5809.
- (21) Koseoglu, Y.; Kavas, H. Size and surface effects on magnetic properties of Fe3O4 nanoparticles. *J. Nanosci. Nanotechnol.* **2008**, 8 (2), 584–590.
- (22) Darbandi, M.; Stromberg, F.; Landers, J.; Reckers, N.; Sanyal, B.; Keune, W.; Wende, H., Nanoscale size effect on surface spin canting in iron oxide nanoparticles synthesized by the microemulsion method *J. Phys. D: Appl. Phys.* **2012**, *45* (19).195001
- (23) Schaller, V.; Wahnstrom, G.; Sanz-Velasco, A.; Gustafsson, S.; Olsson, E.; Enoksson, P.; Johansson, C., Effective magnetic moment of magnetic multicore nanoparticles *Phys. Rev. B* **2009**, *80* (9). DOI: 10.1103/PhysRevB.80.092406
- (24) Tadic, M.; Kralj, S.; Jagodic, M.; Hanzel, D.; Makovec, D. Magnetic properties of novel superparamagnetic iron oxide nanoclusters and their peculiarity under annealing treatment. *Appl. Surf. Sci.* **2014**, 322, 255–264.
- (25) Jun, Y. W.; Seo, J. W.; Cheon, A. Nanoscaling laws of magnetic nanoparticles and their applicabilities in biomedical sciences. *Acc. Chem. Res.* **2008**, *41* (2), 179–189.
- (26) Vreeland, E. C.; Watt, J.; Schober, G. B.; Hance, B. G.; Austin, M. J.; Price, A. D.; Fellows, B. D.; Monson, T. C.; Hudak, N. S.; Maldonado-Camargo, L.; et al. Enhanced nanoparticle size control by extending LaMer's mechanism. *Chem. Mater.* **2015**, 27 (17), 6059–6066.
- (27) Moya, C.; Iglesias-Freire, Ó.; Batlle, X.; Labarta, A.; Asenjo, A. Superparamagnetic versus blocked states in aggregates of Fe 3– x O 4 nanoparticles studied by MFM. *Nanoscale* **2015**, 7 (42), 17764–17770.
- (28) Mourdikoudis, S.; Pallares, R. M.; Thanh, N. T. Characterization techniques for nanoparticles: comparison and complementarity upon studying nanoparticle properties. *Nanoscale* **2018**, *10* (27), 12871–12934.
- (29) Ivanov, A. O.; Kantorovich, S. S.; Zverev, V. S.; Elfimova, E. A.; Lebedev, A. V.; Pshenichnikov, A. F. Temperature-dependent dynamic correlations in suspensions of magnetic nanoparticles in a broad range of concentrations: a combined experimental and theoretical study. *Phys. Chem. Chem. Phys.* **2016**, *18* (27), 18342–18352.
- (30) Yeap, S. P.; Lim, J.; Ooi, B. S.; Ahmad, A. L. Agglomeration, colloidal stability, and magnetic separation of magnetic nanoparticles: collective influences on environmental engineering applications. *J. Nanopart. Res.* **2017**, *19* (11), 1–15.

- (31) Lim, J.; Yeap, S. P.; Che, H. X.; Low, S. C. Characterization of magnetic nanoparticle by dynamic light scattering. *Nanoscale Res. Lett.* **2013**, *8* (1), 1–14.
- (32) Eberbeck, D.; Wiekhorst, F.; Steinhoff, U.; Trahms, L. Aggregation behaviour of magnetic nanoparticle suspensions investigated by magnetorelaxometry. *J. Phys.: Condens. Matter* **2006**, *18* (38), S2829.
- (33) Moore, T. L.; Rodriguez-Lorenzo, L.; Hirsch, V.; Balog, S.; Urban, D.; Jud, C.; Rothen-Rutishauser, B.; Lattuada, M.; Petri-Fink, A. Nanoparticle colloidal stability in cell culture media and impact on cellular interactions. *Chem. Soc. Rev.* **2015**, *44* (17), 6287–6305.
- (34) Lu, Z.; Yin, Y. Colloidal nanoparticle clusters: functional materials by design. Chem. Soc. Rev. 2012, 41 (21), 6874–6887.
- (35) Li, Z.; Fan, Q.; Yin, Y., Colloidal Self-Assembly Approaches to Smart Nanostructured Materials *Chem. Rev.* **2021**. DOI: 10.1021/acs.chemrev.1c00482
- (36) Bender, P.; Fock, J.; Frandsen, C.; Hansen, M. F.; Balceris, C.; Ludwig, F.; Posth, O.; Wetterskog, E.; Bogart, L. K.; Southern, P.; et al. Relating Magnetic Properties and High Hyperthermia Performance of Iron Oxide Nanoflowers. *J. Phys. Chem. C* **2018**, 122 (5), 3068–3077.
- (37) Bender, P.; Fock, J.; Hansen, M. F.; Bogart, K.; Southern, P.; Ludwig, F.; Wiekhorst, F.; Szczerba, W.; Zeng, L. J.; Heinke, D.; et al. Influence of clustering on the magnetic properties and hyperthermia performance of iron oxide nanoparticles. *Nanotechnology* **2018**, 29 (42), 425705.
- (38) Zhuang, J. Q.; Wu, H. M.; Yang, Y. A.; Cao, Y. C. Supercrystalline colloidal particles from artificial atoms. *J. Am. Chem. Soc.* **2007**, *129* (46), 14166.
- (39) Wang, T.; Wang, X. R.; LaMontagne, D.; Wang, Z. L.; Wang, Z. W.; Cao, Y. C. Shape-Controlled Synthesis of Colloidal Superparticles from Nanocubes. *J. Am. Chem. Soc.* **2012**, *134* (44), 18225–18228.
- (40) Bunge, A.; Porav, A. S.; Borodi, G.; Radu, T.; Pîrnău, A.; Berghian-Grosan, C.; Turcu, R. Correlation between synthesis parameters and properties of magnetite clusters prepared by solvothermal polyol method. *J. Mater. Sci.* 2019, 54 (4), 2853–2875.
- (41) Matijevic, E.; Scheiner, P. FERRIC HYDROUS OXIDE SOLS 0.3. PREPARATION OF UNIFORM PARTICLES BY HYDROLYSIS OF FE(III)-CHLORIDE, FE(III)-NITRATE, AND FE(III)-PERCHLORATE SOLUTIONS. J. Colloid Interface Sci. 1978, 63 (3), 509–524.
- (42) Zhang, J.; Song, Y.-F.; Cronin, L.; Liu, T. Self-assembly of organic—inorganic hybrid amphiphilic surfactants with large polyoxometalates as polar head groups. *J. Am. Chem. Soc.* **2008**, *130* (44), 14408–14409.
- (43) Chen, O.; Riedemann, L.; Etoc, F.; Herrmann, H.; Coppey, M.; Barch, M.; Farrar, C. T.; Zhao, J.; Bruns, O. T.; Wei, H. Magneto-fluorescent core-shell supernanoparticles. *Nat. Commun.* **2014**, 5 (1), 1–8.
- (44) Lartigue, L.; Hugounenq, P.; Alloyeau, D.; Clarke, S. P.; Levy, M.; Bacri, J.-C.; Bazzi, R.; Brougham, D. F.; Wilhelm, C.; Gazeau, F. Cooperative organization in iron oxide multi-core nanoparticles potentiates their efficiency as heating mediators and MRI contrast agents. ACS Nano 2012, 6 (12), 10935–10949.
- (45) Ge, J.; Hu, Y.; Biasini, M.; Beyermann, W. P.; Yin, Y. Superparamagnetic magnetite colloidal nanocrystal clusters. *Angew. Chem., Int. Ed.* **2007**, 46 (23), 4342–4345.
- (46) Xi, G.; Wang, C.; Wang, X. The Oriented Self-Assembly of Magnetic Fe3O4 Nanoparticles into Monodisperse Microspheres and Their Use as Substrates in the Formation of Fe3O4 Nanorods. *Eur. J. Inorg. Chem.* **2008**, 2008 (3), 425–431.
- (47) Cheng, C.; Xu, F.; Gu, H. Facile synthesis and morphology evolution of magnetic iron oxide nanoparticles in different polyol processes. *New J. Chem.* **2011**, 35 (5), 1072–1079.
- (48) Cheng, C.; Wen, Y.; Xu, X.; Gu, H. Tunable synthesis of carboxyl-functionalized magnetite nanocrystal clusters with uniform size. *J. Mater. Chem.* **2009**, *19* (46), 8782–8788.
- (49) Wang, L.; Bao, J.; Wang, L.; Zhang, F.; Li, Y. One-pot synthesis and bioapplication of amine-functionalized magnetite nanoparticles

- and hollow nanospheres. Chemistry-A European Journal 2006, 12 (24), 6341-6347.
- (50) Deng, H.; Li, X.; Peng, Q.; Wang, X.; Chen, J.; Li, Y. Monodisperse magnetic single-crystal ferrite microspheres. *Angew. Chem.* **2005**, *117* (18), 2842–2845.
- (51) Narayanaswamy, A.; Xu, H.; Pradhan, N.; Peng, X. Crystalline nanoflowers with different chemical compositions and physical properties grown by limited ligand protection. *Angew. Chem., Int. Ed.* **2006**, *45* (32), 5361–5364.
- (52) Wang, F.; Richards, V. N.; Shields, S. P.; Buhro, W. E. Kinetics and mechanisms of aggregative nanocrystal growth. *Chem. Mater.* **2014**, *26* (1), 5–21.
- (53) Zaiser, E. M.; La Mer, V. K. The kinetics of the formation and growth of monodispersed sulfur hydrosols. *Journal of colloid science* **1948**, 3 (6), 571–598.
- (54) You, H.; Fang, J. Particle-mediated nucleation and growth of solution-synthesized metal nanocrystals: A new story beyond the LaMer curve. *Nano Today* **2016**, *11* (2), 145–167.
- (55) Voorhees, P. W. The theory of Ostwald ripening. *J. Stat. Phys.* **1985**, 38 (1), 231–252.
- (56) Kabalnov, A. Ostwald ripening and related phenomena. *J. Dispersion Sci. Technol.* **2001**, 22 (1), 1–12.
- (57) Gerber, O.; Pichon, B.; Ihiawakrim, D.; Florea, I.; Moldovan, S.; Ersen, O.; Begin, D.; Grenèche, J.-M.; Lemonnier, S.; Barraud, E. Synthesis engineering of iron oxide raspberry-shaped nanostructures. *Nanoscale* **2017**, *9* (1), 305–313.
- (58) Gavilan, H.; Sanchez, E. H.; Brollo, M. E. F.; Asin, L.; Moerner, K. K.; Frandsen, C.; Lazaro, F. J.; Serna, C. J.; Veintemillas-Verdaguer, S.; Morales, M. P.; Gutierrez, L. Formation mechanism of maghemite nanoflowers synthesized by a polyol-mediated process. *ACS Omega* **2017**, *2* (10), 7172–7184.
- (59) Wei, X.; Jing, L.; Liu, C.; Hou, Y.; Jiao, M.; Gao, M. Molecular mechanisms for delicately tuning the morphology and properties of Fe 3 O 4 nanoparticle clusters. *CrystEngComm* **2018**, 20 (17), 2421–2429
- (60) Togashi, T.; Naka, T.; Asahina, S.; Sato, K.; Takami, S.; Adschiri, T. Surfactant-assisted one-pot synthesis of superparamagnetic magnetite nanoparticle clusters with tunable cluster size and magnetic field sensitivity. *Dalton Transactions* **2011**, 40 (5), 1073–1078
- (61) Otero-Lorenzo, R.; Ramos-Docampo, M. A.; Rodríguez-González, B.; Comesaña-Hermo, M.; Salgueiriño, V. n. Solvothermal clustering of magnetic spinel ferrite nanocrystals: a Raman perspective. *Chem. Mater.* **2017**, *29* (20), 8729–8736.
- (62) Lin, M.; Huang, H.; Liu, Z.; Liu, Y.; Ge, J.; Fang, Y. Growth–dissolution–regrowth transitions of Fe3O4 nanoparticles as building blocks for 3D magnetic nanoparticle clusters under hydrothermal conditions. *Langmuir* **2013**, *29* (49), 15433–15441.
- (63) Hemery, G.; Keyes, A. C., Jr; Garaio, E.; Rodrigo, I.; Garcia, J. A.; Plazaola, F.; Garanger, E.; Sandre, O. Tuning sizes, morphologies, and magnetic properties of monocore versus multicore iron oxide nanoparticles through the controlled addition of water in the polyol synthesis. *Inorganic chemistry* **2017**, *56* (14), 8232–8243.
- (64) Kostopoulou, A.; Velu, S. K.; Thangavel, K.; Orsini, F.; Brintakis, K.; Psycharakis, S.; Ranella, A.; Bordonali, L.; Lappas, A.; Lascialfari, A. Colloidal assemblies of oriented maghemite nanocrystals and their NMR relaxometric properties. *Dalton Transactions* **2014**, 43 (22), 8395–8404.
- (65) Maity, D.; Chandrasekharan, P.; Pradhan, P.; Chuang, K.-H.; Xue, J.-M.; Feng, S.-S.; Ding, J. Novel synthesis of superparamagnetic magnetite nanoclusters for biomedical applications. *J. Mater. Chem.* **2011**, *21* (38), 14717–14724.
- (66) Nikitin, A. A.; Shchetinin, I. V.; Tabachkova, N. Y..; Soldatov, M. A.; Soldatov, A. V.; Sviridenkova, N. V.; Beloglazkina, E. K.; Savchenko, A. G.; Fedorova, N. D.; Abakumov, M. A.; Majouga, A. G. Synthesis of iron oxide nanoclusters by thermal decomposition. *Langmuir* **2018**, *34* (15), 4640–4650.

- (67) Xuan, S.; Wang, Y.-X. J.; Yu, J. C.; Cham-Fai Leung, K. Tuning the grain size and particle size of superparamagnetic Fe3O4 microparticles. *Chem. Mater.* **2009**, 21 (21), 5079–5087.
- (68) Huang, Z.; Wu, K.; Yu, Q.-H.; Wang, Y.-Y.; Xing, J.; Xia, T.-L. Facile synthesis of size tunable Fe3O4 nanoparticles in bisolvent system. *Chem. Phys. Lett.* **2016**, *664*, 219–225.
- (69) Liang, J.; Ma, H.; Luo, W.; Wang, S. Synthesis of magnetite submicrospheres with tunable size and superparamagnetism by a facile polyol process. *Mater. Chem. Phys.* **2013**, *139* (2–3), 383–388.
- (70) Liu, J.; Sun, Z.; Yonghui; Zou, Y.; Li, C.; Guo, X.; Xiong, L.; Gao, Y.; Li, F.; Zhao, D. Highly water-dispersible biocompatible magnetite particles with low cytotoxicity stabilized by citrate groups. *Angew. Chem., Int. Ed.* **2009**, *48* (32), 5875–5879.
- (71) Liu, R.; Lv, M.; Wang, Q.; Li, H.; Guo, P.; Zhao, X. Solvothermal synthesis of size-tunable ZnFe2O4 colloidal nanocrystal assemblies and their electrocatalytic activity towards hydrogen peroxide. *J. Magn. Magn. Mater.* **2017**, 424, 155–160.
- (72) Lu, C.; Wang, H.; Ma, J.; Yuan, H.; Liang, H.; Wu, L.; Chai, K. Y.; Li, S. Facile synthesis of superparamagnetic magnetite nanoflowers and their applications in cellular imaging. *RSC Adv.* **2016**, *6* (48), 42649–42655.
- (73) Luo, B.; Song, X.-J.; Zhang, F.; Xia, A.; Yang, W.-L.; Hu, J.-H.; Wang, C.-C. Multi-functional thermosensitive composite microspheres with high magnetic susceptibility based on magnetite colloidal nanoparticle clusters. *Langmuir* **2010**, 26 (3), 1674–1679.
- (74) Pereira, C.; Pereira, A. M.; Rocha, M.; Freire, C.; Geraldes, C. F. Architectured design of superparamagnetic Fe 3 O 4 nanoparticles for application as MRI contrast agents: mastering size and magnetism for enhanced relaxivity. *J. Mater. Chem. B* **2015**, 3 (30), 6261–6273.
- (75) Tong, G.; Liu, Y.; Wu, T.; Tong, C.; Du, F. H 2 O-steered size/phase evolution and magnetic properties of large-scale, monodisperse Fe x O y nanomaterials. *Journal of Materials Chemistry C* **2015**, 3 (21), 5506–5515.
- (76) Wang, T.; Zhang, L.; Wang, H.; Yang, W.; Fu, Y.; Zhou, W.; Yu, W.; Xiang, K.; Su, Z.; Dai, S.; Chai, L. Controllable synthesis of hierarchical porous Fe3O4 particles mediated by poly (diallyldimethylammonium chloride) and their application in arsenic removal. ACS Appl. Mater. Interfaces 2013, 5 (23), 12449–12459.
- (77) Wang, W.; Tang, B.; Ju, B.; Zhang, S. Size-controlled synthesis of water-dispersible superparamagnetic Fe 3 O 4 nanoclusters and their magnetic responsiveness. RSC Adv. 2015, 5 (92), 75292–75299.
- (78) Kim, Y. J.; Park, B. C.; Choi, Y. S.; Ko, M. J.; Kim, Y. K. Quantitative analysis on cellular uptake of clustered ferrite magnetic nanoparticles. *Electronic Materials Letters* **2019**, *15* (4), 471–480.
- (79) Zhu, Y.; Zhao, W.; Chen, H.; Shi, J. A simple one-pot self-assembly route to nanoporous and monodispersed Fe3O4 particles with oriented attachment structure and magnetic property. *J. Phys. Chem. C* **2007**, *111* (14), 5281–5285.
- (80) Xiao, Z.; Zhang, Q.; Guo, X.; Villanova, J.; Hu, Y.; Kulaots, I.; Garcia-Rojas, D.; Guo, W.; Colvin, V. L. Libraries of Uniform Magnetic Multicore Nanoparticles with Tunable Dimensions for Biomedical and Photonic Applications. ACS Appl. Mater. Interfaces 2020, 12 (37), 41932–41941.
- (81) Mørup, S.; Hansen, M. F.; Frandsen, C. Magnetic interactions between nanoparticles. *Beilstein journal of nanotechnology* **2010**, *1* (1), 182–190.
- (82) Sanchez, F. H.; Mendoza Zelis, P.; Arciniegas, M. L.; Pasquevich, G. A.; Fernandez van Raap, M. B. Dipolar interaction and demagnetizing effects in magnetic nanoparticle dispersions: Introducing the mean-field interacting superparamagnet model. *Phys. Rev. B* **2017**, *95* (13), 134421.
- (83) Landeros, P.; Escrig, J.; Altbir, D.; Laroze, D.; d'Albuquerque e Castro, J.; Vargas, P. Scaling relations for magnetic nanoparticles. *Phys. Rev. B* **2005**, *71* (9), 094435.
- (84) Kostopoulou, A.; Brintakis, K.; Vasilakaki, M.; Trohidou, K.; Douvalis, A.; Lascialfari, A.; Manna, L.; Lappas, A. Assembly-mediated interplay of dipolar interactions and surface spin disorder in colloidal maghemite nanoclusters. *Nanoscale* **2014**, *6* (7), 3764–3776.

- (85) Hemery, G.; Genevois, C.; Couillaud, F.; Lacomme, S.; Gontier, E.; Ibarboure, E.; Lecommandoux, S.; Garanger, E.; Sandre, O. Monocore vs. multicore magnetic iron oxide nanoparticles: Uptake by glioblastoma cells and efficiency for magnetic hyperthermia. *Molecular Systems Design & Engineering* **2017**, 2 (5), 629–639.
- (86) Wang, C.; Xu, H.; Liang, C.; Liu, Y. M.; Li, Z. W.; Yang, G. B.; Cheng, H.; Li, Y. G.; Liu, Z. Iron Oxide @ Polypyrrole Nanoparticles as a Multifunctional Drug Carrier for Remotely Controlled Cancer Therapy with Synergistic Antitumor Effect. ACS Nano 2013, 7 (8), 6782–6795.
- (87) Wang, T.; Zhang, L.; Li, C.; Yang, W.; Song, T.; Tang, C.; Meng, Y.; Dai, S.; Wang, H.; Chai, L.; Luo, J. Synthesis of core—shell magnetic Fe3O4@ poly (m-phenylenediamine) particles for chromium reduction and adsorption. *Environ. Sci. Technol.* **2015**, 49 (9), 5654–5662.
- (88) Xia, H.; Zhang, L.; Chen, Q. D.; Guo, L.; Fang, H. H.; Li, X. B.; Song, J. F.; Huang, X. R.; Sun, H. B. Band-Gap-Controllable Photonic Crystals Consisting of Magnetic Nanocrystal Clusters in a Solidified Polymer Matrix. *J. Phys. Chem. C* **2009**, *113* (43), 18542–18545.
- (89) He, L.; Wang, M. S.; Ge, J. P.; Yin, Y. D. Magnetic Assembly Route to Colloidal Responsive Photonic Nanostructures. *Acc. Chem. Res.* **2012**, *45* (9), 1431–1440.
- (90) Kim, H.; Ge, J.; Kim, J.; Choi, S.-e.; Lee, H.; Lee, H.; Park, W.; Yin, Y.; Kwon, S. Structural colour printing using a magnetically tunable and lithographically fixable photonic crystal. *Nat. Photonics* **2009**, *3* (9), 534–540.
- (91) Ge, J. P.; Yin, Y. D. Responsive Photonic Crystals. *Angew. Chem.-Int. Ed.* **2011**, *50* (7), 1492–1522.
- (92) Bagaria, H. G.; Yoon, K. Y.; Neilson, B. M.; Cheng, V.; Lee, J. H.; Worthen, A. J.; Xue, Z.; Huh, C.; Bryant, S. L.; Bielawski, C. W.; Johnston, K. P. Stabilization of iron oxide nanoparticles in high sodium and calcium brine at high temperatures with adsorbed sulfonated copolymers. *Langmuir* **2013**, *29* (10), 3195–3206.
- (93) Bixner, O.; Lassenberger, A.; Baurecht, D.; Reimhult, E. Complete Exchange of the Hydrophobic Dispersant Shell on Monodisperse Superparamagnetic Iron Oxide Nanoparticles. *Langmuir* **2015**, 31 (33), 9198–9204.
- (94) Ding, X.; Vegesna, G. K.; Meng, H.; Winter, A.; Lee, B. P. Nitro-Group Functionalization of Dopamine and its Contribution to the Viscoelastic Properties of Catechol-Containing Nanocomposite Hydrogels. *Macromolecular chemistry and physics* **2015**, 216 (10), 1109–1119.
- (95) Thomas, G.; Demoisson, F.; Chassagnon, R.; Popova, E.; Millot, N. One-step continuous synthesis of functionalized magnetite nanoflowers. *Nanotechnology* **2016**, *27* (13), 135604.
- (96) Yu, W. W.; Chang, E.; Sayes, C. M.; Drezek, R.; Colvin, V. L. Aqueous dispersion of monodisperse magnetic iron oxide nanocrystals through phase transfer. *Nanotechnology* **2006**, *17* (17), 4483–4487.
- (97) Zirbs, R.; Lassenberger, A.; Vonderhaid, I.; Kurzhals, S.; Reimhult, E. Melt-grafting for the synthesis of core-shell nanoparticles with ultra-high dispersant density. *Nanoscale* **2015**, *7* (25), 11216–11225.
- (98) Gleich, B.; Weizenecker, J. Tomographic imaging using the nonlinear response of magnetic particles. *Nature* **2005**, 435 (7046), 1214–1217.
- (99) Bauer, L. M.; Situ, S. F.; Griswold, M. A.; Samia, A. C. Magnetic Particle Imaging Tracers: State-of-the-Art and Future Directions. *J. Phys. Chem. Lett.* **2015**, 6 (13), 2509–17.
- (100) Panagiotopoulos, N.; Duschka, R. L.; Ahlborg, M.; Bringout, G.; Debbeler, C.; Graeser, M.; Kaethner, C.; Ludtke-Buzug, K.; Medimagh, H.; Stelzner, J.; Buzug, T. M.; Barkhausen, J.; Vogt, F. M.; Haegele, J. Magnetic particle imaging: current developments and future directions. *Int. J. Nanomedicine* **2015**, *10*, 3097–114.
- (101) Chandrasekharan, P.; Tay, Z. W.; Zhou, X. Y.; Yu, E.; Orendorff, R.; Hensley, D.; Huynh, Q.; Fung, K. L. B.; VanHook, C. C.; Goodwill, P.; Zheng, B.; Conolly, S.; et al. A perspective on a rapid and radiation-free tracer imaging modality, magnetic particle imaging, with promise for clinical translation. *Br J. Radiol.* **2018**, *91* (1091), 20180326.

- (102) Tay, Z. W.; Hensley, D. W.; Vreeland, E. C.; Zheng, B.; Conolly, S. M. The Relaxation Wall: Experimental Limits to Improving MPI Spatial Resolution by Increasing Nanoparticle Core size. *Biomed Phys. Eng. Express* **2017**, 3 (3), 035003.
- (103) Wu, L. C.; Zhang, Y.; Steinberg, G.; Qu, H.; Huang, S.; Cheng, M.; Bliss, T.; Du, F.; Rao, J.; Song, G.; Pisani, L.; Doyle, T.; Conolly, S.; Krishnan, K.; Grant, G.; Wintermark, M. A Review of Magnetic Particle Imaging and Perspectives on Neuroimaging. *AJNR Am. J. Neuroradiol* **2019**, 40 (2), 206–212.

□ Recommended by ACS

Low-Gradient Magnetophoresis of Nanospheres and Nanorods through a Single Layer of Paper

James Kah Chun Law, JitKang Lim, et al.

MARCH 29, 2023

LANGMUIR

READ 🗹

Crystal-Chemical and Biological Controls of Elemental Incorporation into Magnetite Nanocrystals

Matthieu Amor, Daniel M. Chevrier, et al.

JANUARY 03, 2023

ACS NANO

READ 🗹

Local Temperature Increments and Induced Cell Death in Intracellular Magnetic Hyperthermia

Yuanyu Gu, Angel Millán, et al.

MARCH 20, 2023

ACS NANO

READ

pH Dependence of MRI Contrast in Magnetic Nanoparticle Suspensions Demonstrates Inner-Sphere Relaxivity Contributions and Reveals the Mechanism of Dissolution

Eoghan MacMahon and Dermot F. Brougham

FEBRUARY 03, 2023

LANGMUIR

READ 🗹

Get More Suggestions >